

Discovery of X-ray Emission from the Wolf-Rayet star WR 142 of oxygen subtype

L. M. Oskinova, W.-R. Hamann, A. Feldmeier

Institute for Physics and Astronomy, University Potsdam, 14476 Potsdam, Germany

`lida@astro.physik.uni-potsdam.de`

R. Ignace

Department of Physics and Astronomy, East Tennessee State University, Johnson City, TN 37614, USA

Y.-H. Chu

Department of Astronomy, University of Illinois, 1002 West Green Street, Urbana, IL 61801, USA

ABSTRACT

We report the discovery of weak yet hard X-ray emission from the Wolf-Rayet (WR) star WR 142 with the *XMM-Newton* X-ray telescope. Being of spectral subtype WO2, WR 142 is a massive star in a very advanced evolutionary stage, short before its explosion as a supernova or γ -ray burst. This is the first detection of X-ray emission from a WO-type star. We rule out any serendipitous X-ray sources within $\approx 1''$ of WR 142. WR 142 has an X-ray luminosity of $L_X = 7 \times 10^{30} \text{ erg s}^{-1}$, which constitutes only $\lesssim 10^{-8}$ of its bolometric luminosity. The hard X-ray spectrum suggests a plasma temperature of about 100 MK. Commonly, X-ray emission from stellar winds is attributed to embedded shocks due to the intrinsic instability of the radiation driving. From qualitative considerations we conclude that this mechanism cannot account for the hardness of the observed radiation. There are no hints for a binary companion. Therefore the only remaining, albeit speculative explanation must refer to magnetic activity. Possibly related, WR 142 seems to rotate extremely fast, as indicated by the unusually round profiles of its optical emission lines. Our detection implies that the wind of WR 142 must be relatively transparent to X-rays, which can be due to strong wind ionization, wind clumping, or non-spherical geometry from rapid rotation.

Subject headings: stars: winds, outflows — stars: Wolf-Rayet — stars: individual (WR 142) — X-rays: stars

1. Introduction

Stars of the Wolf-Rayet (WR) type have a highly peculiar chemical composition and very strong stellar winds. The WR spectra are sorted into three subclasses: WN, WC, and WO, according to the dominance of nitrogen, carbon, and oxygen emission lines, respectively. These spectral types correspond to evolutionary stages (Conti et al. 1983). The largest C+O abundance and the fastest stellar winds are observed in WO

type stars, that represent the final evolutionary stage of a massive star prior to its explosion as a type Ic supernova or γ -ray burst (Hirschi et al. 2005).

The WR stars continue to challenge our understanding of line-driven winds. Schaerer (1996) pointed out the importance of the iron opacity for the acceleration of WR winds. The first hydrodynamical model for a WR wind was presented by Gräfener & Hamann (2005). In their simulation

the mass loss is initiated at high optical depth by the so-called “iron bump” in the opacity. It was thus demonstrated that WR-type winds can be driven by radiation pressure.

It has long been known that line-driven winds are subject to an instability that can lead to strong shocks (Lucy & White 1980). These shocks are thought to explain the X-ray emissions from O star winds, as predicted by time-dependent hydrodynamic modeling (Owocki et al. 1988; Feldmeier et al. 1997) and largely confirmed by observations (Kramer et al. 2003; Oskinova et al. 2006; Zhekov & Palla 2007; Waldron & Cassinelli 2007). The growth of instability in WR winds was investigated by Gayley & Owocki (1995). They found that despite of damping effects due to the multi-line scattering, the instability remains effective. Therefore, X-ray emission from wind shocks could, in principle, be expected in WR winds, a conjecture that has not been yet tested by time-dependent hydrodynamic simulations.

Significant observational effort has been made to study the X-ray emission of WR stars. White & Long (1986), Pollock (1987), Pollock et al. (1995), Oskinova (2005) presented X-ray observations of Galactic WR stars. A survey of X-ray emission from WR stars in the Magellanic Clouds was conducted by Guerrero & Chu (2008a,b). Ignace et al. (2000) and Oskinova (2005) demonstrated that X-ray properties of single WR stars differ from those of O stars. Whereas O stars display a trend in which the ratio of the X-ray to the bolometric luminosity L_X/L_{bol} has a typical value of 10^{-7} (Long & White 1980; Berghoefer et al. 1997; Sana et al. 2006), this trend is not observed in the case of WR stars.

Observations with the *XMM-Newton* and *Chandra* X-ray telescopes established that some bona fide single WN stars are X-ray active (Skinner et al. 2002a,b; Ignace et al. 2003; Oskinova 2005), while others are apparently not (Oskinova 2005; Gosset et al. 2005). Oskinova et al. (2003) found that no single WC star had been conclusively detected at X-ray energies, a result that continues to hold. Among the WR subclasses, only the WO-type stars have not been observed in X-rays so far. In this *Letter* we present the *XMM-Newton* observations of the closest WO type star WR 142. The star is introduced in Sect. 2, and its *XMM-Newton* observations are described in Sect. 3. The impli-

cations of the *XMM-Newton* detection of WR 142 are discussed in Sect. 4.

2. The WO-type Star WR 142

WR 142, also named Sand 5 and St 3, has a spectrum characteristic for the spectral subtype WO2 (Barlow & Hummer 1982; Kingsburgh et al. 1994). The optical spectrum of WR 142 was discussed by Polcaro et al. (1997), who also noticed some line variability.

Figure 1 shows the spectral energy distribution (SED) of WR 142 together with model calculated with the Potsdam Wolf-Rayet (PoWR) model atmosphere code (Gräfener et al. 2002). Photometric IR measurements are plotted together with our optical spectrum and the *Spitzer* IRS mid-IR spectrum. We have adopted parameters typical for a WO star: stellar temperature $T_* = 150$ kK, “transformed radius” (cf. Gräfener et al. 2002) $R_t = 2R_\odot$, and a composition of 40% carbon, 30% oxygen and 30% helium (by mass). WR 142 is assumed to be a member of the open cluster Berkeley 87 at a distance of $d = 1.23$ kpc (Turner et al. 2006). Based on this preliminary model, the fit of the photometric observations requires an interstellar reddening of $E_{B-V} = 1.7$ mag and a stellar luminosity of $\log L_{\text{bol}}/L_\odot = 5.35$, implying a stellar radius of only $R_* = 0.6 R_\odot$. The corresponding mass-loss rate is about $10^{-5.1} M_\odot \text{yr}^{-1}$ for an adopted microclumping volume filling factor of 0.1.

The adopted model does not provide an entirely satisfactory fit to the line spectra. For example, the model does not match the huge O VI emission at 3811, 3834 Å, a problem also experienced by Crowther et al. (2000) while reproducing these lines for Sand 2 with the CMFGEN code. We also fitted the SED shown in Fig. 1 with a model that has a mass-loss rate lower by a factor of two, $10^{-5.4} M_\odot \text{yr}^{-1}$, and higher bolometric luminosity, $\log L_{\text{bol}}/L_\odot = 5.65$. This model fits the SED in Fig. 1 equally well. Figure 2 shows the radius of unity optical depth plotted as function of wavelength in the X-ray range for both models. The stronger wind is opaque even to hard X-rays, but the thinner wind is largely transparent, because its higher ionization reduces the X-ray absorbing ions. The same could happen in denser, but hotter models. Thus our ability to predict the influence

of wind photo-absorption is somewhat limited, owing to ambiguities in the ionization state of metals and uncertainty in the mass-loss rate.

The profiles of the emission lines in the spectrum of WR142 are very broad. Assuming that the line widths correspond to the wind terminal velocity, the velocity of $v_\infty \approx 5500 \text{ km s}^{-1}$ would be deduced. However, the profile shapes of almost all lines are much more round than the roughly Gaussian shapes usually seen in WR spectra. Such round profiles cannot be reproduced by the standard models. It is tempting to reproduce these profiles by convolution with the semi-ellipse for rotational broadening, albeit rotating stellar winds certainly require a more sophisticated treatment which has not been accomplished yet. If rotation is the cause for the round profiles, the projected rotation speed must be comparable to v_∞ , i.e. the star would rotate near to break-up with $v_{\text{rot}} \sin i \lesssim 4000 \text{ km s}^{-1}$ (see inset in Fig. 1). Interestingly, a similar suggestion has been made for the hottest and the most compact Galactic WN star, WR 2, ($T_* = 140 \text{ kK}$, $R_* = 0.89 R_\odot$, $v_{\text{rot}} \sin i \approx 2000 \text{ km s}^{-1}$) (Hamann et al. 2006).

3. Observations

WR 142 was observed by *XMM-Newton* during two consecutive satellite orbits (ObsId 0550220101 and ObsId 0550220201). The data were merged and analyzed using the latest versions of software SAS 8.0.0. After the high background level time intervals have been rejected, the combined exposure time of all detectors was $\approx 100 \text{ ks}$; an EPIC image of WR 142 and its surroundings is shown in Fig. 3. WR 142 is detected with a 5σ confidence level in all *XMM-Newton* EPIC detectors using standard source-detection algorithms. We define a ‘‘hardness ratio HR’’ as $\text{HR} = (N_{\text{hard}} - N_{\text{soft}}) / (N_{\text{hard}} + N_{\text{soft}})$, where N_{soft} is the number of counts in the 0.25–2.0 keV band and N_{hard} in the 2.0–12.0 keV band. For WR 142 we find $\text{HR} \approx 0.57$. For comparison, the hardness ratio of the WN star WR 1, which has a reddening similar to WR 142, is $\text{HR}(\text{WR 1}) \approx -0.9$, while more reddened WR 110 has $\text{HR}(\text{WR 110}) \approx -0.4$ and less reddened WR 6 has $\text{HR}(\text{WR 6}) \approx -0.6$. Thus X-ray emission from WR 142 is the hardest among putatively single WR stars. The count rates in the 0.25 keV–

12.0 keV band are $(1.89 \pm 0.34) \times 10^{-3} \text{ c s}^{-1}$ for EPIC MOS1+2 and $(3.80 \pm 0.84) \times 10^{-3} \text{ c s}^{-1}$ for EPIC PN cameras. Assuming a two-temperature thermal plasma model ($kT_1 = 0.3 \text{ keV}$, $kT_2 = 10 \text{ keV}$), the observed X-ray flux of WR 142 is $F_X = 4 \pm 2 \times 10^{-14} \text{ erg s}^{-1} \text{ cm}^{-2}$. The reddening towards WR 142 is known from the analysis of its optical spectrum, and the distance is known from its cluster membership. The X-ray luminosity of WR 142 is thus $L_X \approx 7 \times 10^{30} \text{ erg s}^{-1}$, or $\log L_X / L_{\text{bol}} \approx -8$.

The angular resolution of *XMM-Newton* is $\lesssim 6''$. To exclude the potential confusion with a source in close vicinity of WR 142, we inspected optical and infra-red images with higher angular resolution. According to the USNO-B1.0 catalog (Monet et al. 2003), the closest object to WR 142 is located $8''$ away. The optical monitor (OM) on board of *XMM-Newton* provides images with an angular resolution of $\approx 1''$. The OM images in four filters did not detect any objects closer than $8''$ around WR 142. The *Spitzer* space telescope has observed the Berkeley 87 cluster in the infra-red (IR). With an angular resolution of $\lesssim 1''$, the *Spitzer* IRAC camera took images in four channels. No point sources within $8''$ from WR 142 were detected in any of the IRAC channels. It is extremely unlikely that any X-ray source is not detectable in either the optical or IR. We therefore rule out any serendipitous X-ray sources within $\approx 1''$ of WR 142 that might get confused as our target.

In addition, there is no evidence to suggest that the observed X-rays originate from a wind blown bubble around WR 142. Although theoretically expected, there is a dearth of WR stars with detected diffuse X-ray emission from their wind-blown bubbles (Chu et al. 2003; Wrigge et al. 2005). The only two detected hot bubbles show a limb-brightened morphology and are extended on the scale of parsecs. On the contrary, we confidently detect a point source at the position of WR 142.

The spectra of WR 142 were extracted from the $15''$ region. The small number of counts obtained in our observation does not allow for quantitative spectral analysis, but interesting conclusions can be made about the gross energy distribution. Figure 4 shows the X-ray spectrum of WR 142 before a background subtraction, together with the spec-

trum of a nearby background region normalized to the same area. The emission from WR 142 dominates over the background at $2 - 7 \text{ \AA}$ ($1.7 - 6 \text{ keV}$), while longwards it dives below the background until about $\approx 20 \text{ \AA}$ (0.6 keV) where it rises above the background again. The presence of “a dip” between $\approx 7 - 12 \text{ \AA}$ ($0.8 - 1 \text{ keV}$) is also seen in the background-subtracted PN and MOS-2 spectra shown in Fig. 5. The appearance of the dip may be due to unresolved strong emission lines. However, the wavelength of the dip coincides well with the K-shell edges of oxygen (Verner & Yakovlev 1995), where our stellar wind models predict an absorption *maximum* (see Fig. 2). Therefore it is tempting to attribute the observed dip to the oxygen K-shell absorption – to confirm this identification, data of higher quality will be required. Assuming the presence of K-shell of oxygen, the thermal plasma model fit to our low S/N data indicates presence of plasma with temperatures spanning from 1 MK to 100 MK.

4. On The Origin of X-ray Emission from WR 142

The confident detection of weak hard X-rays from WR 142 prompts us to re-consider the previous non-detections of X-ray emission from WR stars. The X-ray luminosity of WR 142 of $L_X \approx 7 \times 10^{30} \text{ erg s}^{-1}$ is comparable to present upper limits for the non-detections (Oskinova et al. 2003; Oskinova 2005; Gosset et al. 2005; Skinner et al. 2006). Perhaps some WR stars that are yet undetected in X-rays may be weak sources similar to WR 142. This raises the question, what is the mechanism responsible for the generation of X-rays in WR stars? Usual suspects are wind shocks and magnetic fields.

The strong-shock condition predicts the peak temperature in the shocked gas, T_X , as

$$kT_X^{\text{max}} = \frac{3}{16} \mu m_H U^2, \quad (1)$$

where U is the velocity with which the gas rams into the shock (i.e., pre-shock velocity relative to the shock), and μ is the mean molecular weight per particle in the *post-shock* gas. As the shock temperatures are very high, abundant species will be nearly entirely ionized. Therefore, μ depends only weakly on chemical compositions. For example,

$\mu \approx \frac{1}{2}$ for ionized H, while for fully ionized carbon, $\mu \approx \frac{2}{3}$. Thus, differences in wind molecular weight between O and WR stars cannot strongly affect the temperatures of the shocked plasma in stars of these types.

Note that Eq. (1) gives an upper limit to the temperature at the shock. Radiative cooling will restrict the hottest temperatures to a limited part of the total emission measure. Moreover, some fraction of the energy will be consumed by ionization processes. To roughly estimate the energy required to ionize WO wind material in the post-shock zone we consider oxygen and assume that the leading ion in the pre-shock material is O VI, while in the post-shock plasma it is O IX. A WO wind may contain 30% of oxygen. The ionization potentials are $\text{IP}(\text{O VI}) \approx 0.14 \text{ keV}$, $\text{IP}(\text{O VII}) \approx 0.74 \text{ keV}$, and $\text{IP}(\text{O VIII}) \approx 0.87 \text{ keV}$ (Cox 2000). The specific energy for ionization is $\epsilon = \Sigma N_i \text{IP}_i$, where $N_i = X_i (A_i m_H)^{-1}$ with X_i being the mass fraction of the element, A_i its atomic weight, and m_H the atomic mass unit. Inserting these numbers, the full ionization of oxygen requires $\epsilon \approx 3 \times 10^{13} \text{ erg g}^{-1}$. This is small compared to the kinetic energy of the wind ($5 \times 10^{15} \text{ erg g}^{-1}$ for typical 1000 km s^{-1}). Thus the ionization is not a significant cooling process even in metal-rich winds.

In the time-dependent hydrodynamic simulations by Feldmeier et al. (1997) the velocity jump U depends on the ratio between the period of the perturbations at the wind base, T_c , and the flow time, $T_{\text{flow}} = R_*/v_\infty$. The former was estimated by the acoustic cut-off period, $T_c = aH^{-1}$, where a is thermal speed and H is the pressure scale height. Assuming that the perturbation are seeded in the hydrostatic layers within the star, $T_c/T_{\text{flow}} \propto a v_{\text{esc}}^{-1}$. The thermal speed is lower in hydrogen-deficient WR atmospheres, while v_{esc} can be larger than in O stars, as it is the case for our program star WR 142. Therefore, the velocity jumps in WR wind shocks are expected to be rather *smaller* than larger, compared to O-star winds.

These qualitative considerations indicate that if the same shock mechanism were in operation in WR and O star winds, the X-ray spectra from WR stars would be softer than those of O stars. However, observations show the contrary – the handful of single WR stars with available spectral measurements all show X-ray emission harder than

typically found in O stars (Skinner et al. 2002a,b; Ignace et al. 2003). This trend is confirmed by our new data on WR 142.

Relatively hard X-ray emission can occur in a binary system; however, optical spectra of WR 142 show no contamination from an early-type companion. A low-mass coronal companion to this initially very massive star is extremely unlikely (Lucy 2006).

Babel & Montmerle (1997) proposed that if a stellar wind is magnetically confined it can be strongly heated. The magnetic field locally dominates the bulk motions if the magnetic energy density exceeds the wind kinetic energy density, $B^2/\mu_0 > \rho v^2$. At characteristic distance of $1 R_*$ from the photosphere, the velocity is $v \approx 0.5v_\infty \approx 2000 \text{ km s}^{-1}$, density $\rho = \dot{M}/4\pi v(r)^2 r \approx 1 \times 10^{-10} \text{ g cm}^{-3}$. Therefore, $B(r = 2R_*) > 7 \text{ kG}$ is required to control the WR 142 wind. For a dipole field, this implies that the magnetic field strength at the surface is larger than 50 kG. A field of such strength is not unrealistic, since the radius of WR 142 is ~ 50 times smaller than that of OB supergiants, where surface fields of 100 G have been observed (Bouret et al. 2008). One may speculate that even less strong magnetic fields may lead to hard X-rays due to some type of reconnection and heating processes as invoked to explain the high X-ray temperatures observed in O type stars (Waldron & Cassinelli 2007).

It is difficult to test where in the wind the observed X-rays have been produced. Since no high-resolution X-ray spectrum of a single WR star exists, the $f-i-r$ emission-line diagnostic that has been used for O-star winds has not been applied to WR stars. X-rays produced close to the stellar core must travel through the bulk of photo-absorbing wind. Tentative evidences for absorption edges are found in the X-ray spectra of WR 1 (Ignace et al. 2003) and WR 142.

In the wind of WR 142, the radius at which the photo-absorption to X-rays is equal to unity is plotted in Fig. 2 against photon energy. The two shown models reproduce the stellar SED equally well. One of the models is thick to X-rays for 1000's of R_* , and the observed X-rays would have to emerge from the far outer regions of the wind. Origin of X-rays far out in the wind is favored in the alternative scenario of X-ray emission from O stars (Pollock 2007). However, a reduction in

the mass-loss (a poorly constrained parameter) by a factor of only two and/or a higher effective stellar temperature result in a higher degree of wind ionization. In this case a fraction of X-rays formed deep in the wind could freely escape. Wind clumping can further reduce wind attenuation (Feldmeier et al. 2003).

There is suggestive evidence that WR 142 is a fast rotator, as is the case for the WN2 star WR 2 (see Sect. 2). The detection of strong and hard ($\log L_X \approx 10^{32} \text{ erg s}^{-1}$, $T_X \gg 10 \text{ MK}$) X-rays in WR 2 (Skinner et al. 2008) likely indicates that a similar mechanism operates in these hot, compact, fast rotating stars. The lower X-ray luminosity of WR 142 compared to WR 2 can reflect the higher absorption of X-rays in its denser wind. Fast rotation can lead to a slow equatorial wind with enhanced density, possibly forming an out-flowing disk, and a faster, thinner polar wind (Ignace et al. 1996). If the round shape of the line profiles found in both, WR 142 and WR 2, is due to rotational broadening, the inclination angle must be large.

Summarizing, we have reported the detection of weak, but hard X-rays from WR 142 and speculate that their origin is connected with magnetic activity of this far-evolved, compact WR star. The specific shape of its optical line profiles signals that WR 142 may be rotating at nearly break-up velocity. In this case the spherical symmetry will be broken, potentially affecting the X-ray production and absorption. Observations of better quality and progress in modeling are certainly needed to understand fully the high-energy processes in the winds of massive stars at late stages of their evolution.

Based on observations obtained with *XMM-Newton*, an ESA science mission with instruments and contributions directly funded by ESA Member States and NASA. This research has made use of NASA's Astrophysics Data System Service and the SIMBAD database, operated at CDS, Strasbourg, France. Special thanks to Robert Gruendl for providing the IR measurements. The authors thank the referee M. De Becker for important comments that improved the paper. Funding for this research has been provided by NASA grant NNX08AW84G (Y-HC and RI) and DLR grant 50 OR 0804 (LMO).

REFERENCES

- Babel, J., & Montmerle, T. 1997, *A&A*, 323, 121
- Barlow, M. J., & Hummer, D. G. 1982, in *IAU Symp. 99, Wolf-Rayet Stars: Observations, Physics, Evolution*, ed. C. W. H. de Loore & A. J. Willis (Dordrecht: Reidel), 387
- Berghoefer T. W., Schmitt J. H. M. M., Danner R., Cassinelli J. P. 1997, *A&A*, 322, 167
- Bouret, J.-C., et al. 2008, *MNRAS*, 389, 75
- Chu, Y.-H., Guerrero, M. A., Gruendl, R. A., Garca-Segura, G., & Wendker, H. L. 2003, *ApJ*, 599, 1189
- Conti, P. S. et al. 1983, *ApJ*, 274, 302
- Cox, A. N. 2000, *Allen's Astrophysical Quantities* (New York: Springer), 527
- Crowther, P. A, et al. 2000, *ApJL*, 538, L51
- Feldmeier, A., Puls, J., & Pauldrach, A. W. A. 1997, *A&A*, 322, 878
- Feldmeier, A., Oskinova, L. M., Hamann, W.-R. 2003, *A&A*, 403, 217
- Gayley, K. G., & Owocki, S. P. 1995, *ApJ*, 446, 801
- Gosset, E., et al. 2005, *A&A*, 429, 685
- Gräfener, G., & Hamann, W.-R. 2005, *A&A*, 432, 633
- Gräfener, G., Koesterke, L., Hamann, W.-R. 2002, *A&A*, 387, 244
- Guerrero, M. A., & Chu, Y.-H. 2008a, *ApJS*, 177, 216
- Guerrero, M. A., & Chu, Y.-H. 2008b, *ApJS*, 177, 238
- Hamann, W.-R., Gräfener, G., Liermann, A. 2006, *A&A*, 457, 1015
- Ignace, R., Cassinelli, J. P., & Bjorkman, J. 1996, *ApJ*, 459, 671
- Ignace, R., Oskinova, L. M., & Foullon, C. 2000, *MNRAS*, 318, 214
- Ignace, R., Oskinova, L. M., & Brown, J. C. 2003, *A&A*, 408, 353
- Hirschi, R., Meynet, G., & Maeder, A. 2005, *A&A*, 443, 581
- Kingsburgh, R. L., Barlow, M. J., & Storey, P. J. 1994, *A&A*, 295, 75
- Kramer R. H., Cohen D. H., & Owocki S. P. 2003, *ApJ*, 592, 532
- Long, K. S., & White, R. L. 1980, *ApJ*, 239, L65
- Lucy, L. B., & White, R. L. 1980, *ApJ*, 241, 300
- Lucy, L. B. 2006, *A&A*, 457, 629
- Monet, D. G., et al. 2003, *AJ*, 125, 984
- Oskinova, L. M., Ignace, R., Hamann, W.-R., Pollock, A. M. T., & Brown, J. C. 2003, *A&A*, 402, 755
- Oskinova, L. M. 2005, *MNRAS*, 361, 679
- Oskinova, L. M., Feldmeier, A., & Hamann, W.-R. 2006, *MNRAS*, 372, 313
- Owocki, S. P., Castor, J. I. & Rybicki, G. B. 1988, *ApJ*, 335, 914
- Polcaro, V. F.; Viotti, R.; Rossi, C.; Norci, L. 1997, *A&A*, 325, 178
- Pollock, A. M. T. 1987, *ApJ*, 320, 283
- Pollock, A. M. T., Haberl, F., & Corcoran, M. F. 1995 1995, in *IAU Symp. 163, Wolf-Rayet Stars: Binaries, Colliding Winds, Evolution*, ed. K. A. van der Hucht & P. M. Williams (Dordrecht: Kluwer), 512
- Pollock, A. M. T. 2007, *A&A*, 463, 1111
- Sana, H., Rauw, G., Nazé, Y., Gosset, E., & Vreux, J.-M. 2006, *MNRAS*, 372, 661
- Skinner, S. L., Zhekov, S. A., Güdel, M., & Schmutz, W. 2002a, *ApJ*, 572, 477
- Skinner, S. L., Zhekov, S. A., Güdel, M., & Schmutz, W. 2002b, *ApJ*, 579, 764
- Skinner, S., Güdel, M., Schmutz, W., & Zhekov, S. 2006, *Ap&SS*, 304, 97

- Skinner, S., Zhekov, S., Güdel, M., Schmutz, W., Sokal, K.R. 2008, in Hot Massive Stars. A life time of influence. International Workshop, Lowell Observatory, October 12-15, 2008. Published electronically.
- Schaerer, D. 1996, *A&A*, 309, 129
- Turner, D. G., Rohanizadegan, M., Berdnikov, L. N., Pastukhova, E. N. 2006, *PASP*, 118, 1533
- Verner, D. A., & Yakovlev, D. G. 1995, *A&AS*, 109, 125
- Waldron, W. L., & Cassinelli, J. P. 2001, *ApJ*, 548
- Waldron, W. L., & Cassinelli, J. P. 2007, *ApJ*, 668, 456
- White, R. L., & Long, K. S. 1986, *ApJ*, 310, 832
- Wrigge, M., Chu, Y-H., Magnier, E. A., & Wendker, H. J. 2005, *ApJ*, 633, 248
- Zhekov, S. A., & Palla, F. 2007, *MNRAS*, 382, 1124

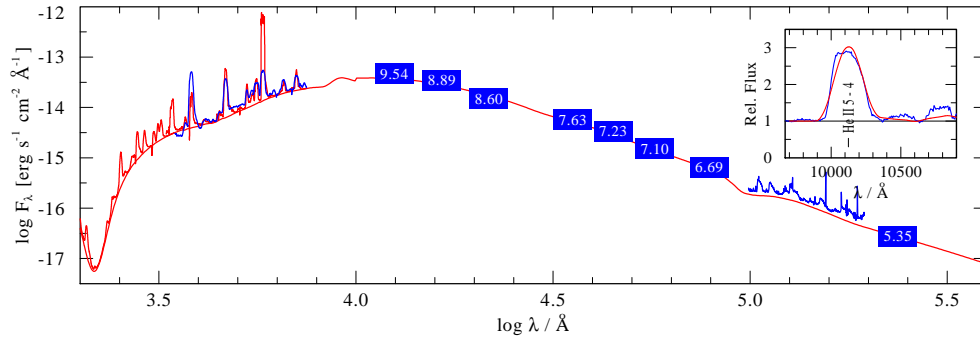


Fig. 1.— Spectral energy distribution of WR 142. Boxes give observed 2MASS, *Spitzer* IRAC and MIPS magnitudes (labels). Observed optic and IR spectra are shown by thin blue lines. The red line is the continuum flux (plus lines in the UV and optical) from a PoWR model with $\log L/L_{\odot} = 5.35$, $T_{*} = 160\text{kK}$, $\dot{M} = 10^{-5.1}M_{\odot}\text{yr}^{-1}$ reddened with $E_{B-V} = 1.73$ mag. The model with $\log L/L_{\odot} = 5.65$ and $\dot{M} = 10^{-5.4}M_{\odot}\text{yr}^{-1}$ gives an equally good fit. A typical He II line is shown in the inset to illustrate the effect of extreme rotational broadening – the observed line (blue) is compared to the synthetic line convolved with $v \sin i = 4000 \text{ km s}^{-1}$ (red).

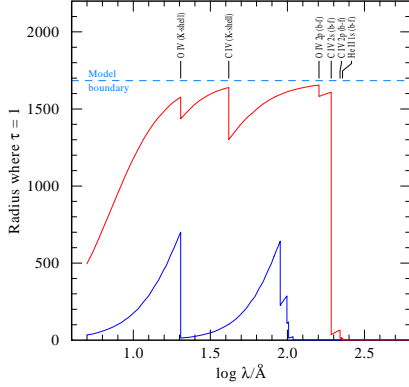


Fig. 2.— Radius (in units of R_*) where the radial optical depth becomes unity, as a function of wavelength in the X-ray range. The red curve is for the same model for which the spectral energy is shown in Fig.1, while the blue curve is for a model with half the mass-loss rate and otherwise similar parameters.

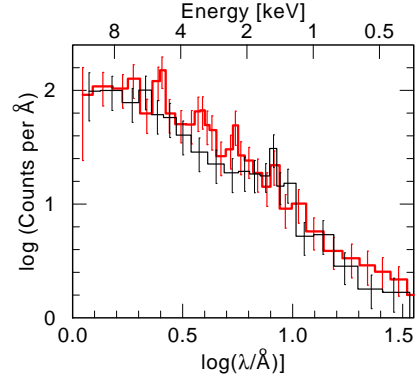


Fig. 4.— Thick red line: *XMM-Newton* MOS-2 spectrum of WR 142 where background has *not* been subtracted. Thin blackline: MOS-2 spectrum of a background region. The error bars give 2σ .

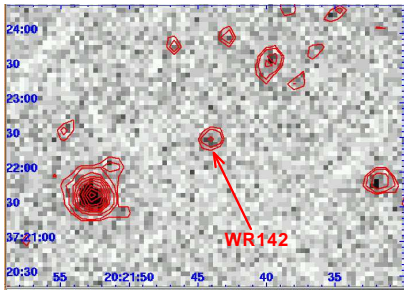


Fig. 3.— Part of the merged *XMM-Newton* EPIC image (0.2-12.0 keV) with over-plotted contours. Image size is $5.7' \times 4.1'$. WR 142 is marked by an arrow. The coordinates are equatorial (J2000). North up, east left.

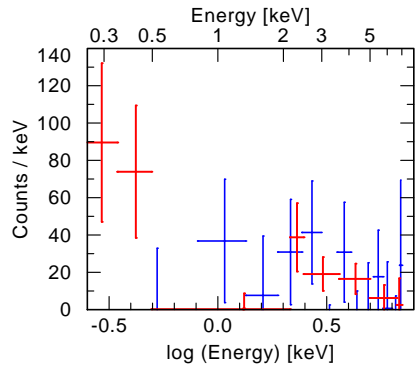


Fig. 5.— *XMM-Newton* MOS-2 (red) and PN (blue) spectra of WR 142 with subtracted background. The error bars give 2σ